High-power red, orange, and green Pr^{3+}:$LiYF_4$ lasers

Philip Werner Metz,[1,*] Fabian Reichert,[1] Francesca Moglia,[1] Sebastian Müller,[1] Daniel-Timo Marzahl,[1] Christian Kränkel,[1,2] and Günter Huber[1,2]

[1]*Institute of Laser-Physics, University of Hamburg, Luruper Chaussee 149, 22761 Hamburg, Germany*

[2]*The Hamburg Centre for Ultrafast Imaging, University of Hamburg, Luruper Chaussee 149, 22761 Hamburg, Germany*

**Corresponding author: Philip.Metz@physnet.uni-hamburg.de*

Received February 26, 2014; revised April 14, 2014; accepted April 15, 2014; posted April 16, 2014 (Doc. ID 207192); published May 23, 2014

Laser experiments with Pr^{3+}:$LiYF_4$ under excitation with a frequency doubled optically pumped semiconductor laser emitting 5 W at 479 nm were performed at seven different laser wavelengths of 523, 546, 604, 607, 640, 698, and 720 nm. At all these wavelengths the output power exceeded 1 W. The best performance at 523 nm with an output power of 2.9 W at a slope efficiency of 72% and an optical-to-optical efficiency of 67% with respect to the incident pump power represents the highest efficiency ever reported for a praseodymium-doped laser material.

OCIS codes: (140.3460) Lasers; (140.7300) Visible lasers; (140.5680) Rare earth and transition metal solid-state lasers.
http://dx.doi.org/10.1364/OL.39.003193

Lasers emitting in the visible spectral region have always attracted a lot of interest. This is not only due to the fascinating look of powerful coherent light beams, which find applications in the entertainment industry, but also and especially because such lasers are valuable instruments in science. They can serve as excitation sources with high photon energies for spectroscopic investigations; combined with the high beam quality and compact dimensions of typical solid state lasers, interest has grown for confocal fluorescence microscopy with high spatial resolution [1]. In industry, visible high-power lasers could open access to precise and efficient processing of metals such as copper or gold, which have a high reflectivity in the infrared spectral range [2].

The first laser, Mayman's flash lamp excited ruby laser [3], emitted at 695 nm in the visible. In the following years lasers based on the trivalent praseodymium ion, which likewise provides several transitions in the visible (see Fig. 1), were demonstrated. Excited by flash lamps as well, these cryogenically cooled lasers emitted initially at 1047 nm in the infrared [4], but shortly after also in the visible at 599 nm [5]. Room temperature operation was enabled by resonantly pumping stoichiometric $PrCl_3$ and $PrBr_3$ using blue pulsed dye lasers [6].

With the development of powerful continuous wave (cw) blue argon ion lasers and frequency doubled neodymium ground state lasers, the Pr^{3+} ion experienced a first revival in the 1990s. Using these pump sources, the first cw lasers based on Pr^{3+}-doped fluoride and oxide crystals in the green, orange, red, and dark red spectral range [7–9] as well as the first mode locking results [10,11] were demonstrated. Moreover, investigations on upconversion pumping schemes with [12–14] and without [15] codopants resulted in visible laser operation of praseodymium in bulk and fiber host materials.

However, it was not until 2004, with the development of directly blue emitting laser diodes around 445 nm based on InGaN [16], that access opened to resonant diode pumping of visible emitting praseodymium lasers. The first directly diode-pumped visible praseodymium laser emitted at 640 nm [17]. Soon after reports on many other transitions in the visible spectral range followed [18–20].

Even today, the available output power from InGaN-based laser diodes is limited to about 1.5 W. Therefore, another semiconductor-based approach for pump sources has attracted attention: frequency doubled optically pumped semiconductor lasers (2ω-OPSL, also known as vertical external-cavity surface-emitting lasers [21]) are commercially available with output powers up to 5 W in the blue spectral range [22]. These devices rely on an InGaAs gain medium in thin disk geometry [23] generating radiation around 960 nm, which is intracavity frequency doubled to about 480 nm. This wavelength allows for efficient resonant pumping of Pr^{3+} ions directly into the emitting $^3P_0$ manifold in various hosts, with the additional advantage of the longer wavelength of 2ω-OPSLs compared to InGaN-laser diodes resulting in a higher Stokes efficiency and a decreased heat generation.

The first 2ω-OPSL-pumped praseodymium lasers utilized Pr:ZBLAN fibers [24] and Pr^{3+}:$LiYF_4$ [25] as gain materials. To date 2ω-OPSLs have been successfully applied for high-power Pr^{3+}-laser operation with more than 4 W of output power in the green spectral range [26], as well as for efficient oxide [27] and waveguide lasers [28,29].

All these results prove the suitability of trivalent praseodymium as an active ion for the generation of coherent visible light. Meanwhile, efficient laser operation

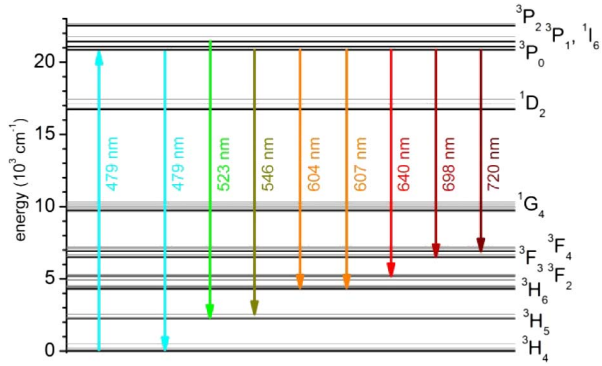

Fig. 1. Energy level scheme and selected transitions of Pr^{3+}:$LiYF_4$.

at a variety of different wavelengths from the blue over the green and orange to the deep red spectral region [30–32] (see Fig. 1), as well as at infrared transitions [4,7], has been realized in various hosts [8,33–35]. Broad band wavelength tuning could be demonstrated covering large parts of the visible spectral range [36,37]. Considering this versatility it seems appropriate to claim praseodymium to be the "neodymium of the visible." However, the efficiencies of Pr^{3+} lasers are often significantly below those of typical Nd^{3+} lasers [38]. Up to now, there are no reports on slope efficiencies exceeding 64% and optical-to-optical efficiencies higher than 60% [39]. Moreover, in these cases the output power was limited to 1 W. So far, the best results were obtained with Pr^{3+}:$LiYF_4$. Due to the higher bandgap of fluorides compared to oxide materials, single- or multiphoton absorption processes of visible photons into the conduction band become unlikely even for high intracavity powers. Additionally, the low phonon cutoff frequency of fluorides effectively suppresses nonradiative multiphonon relaxation processes depopulating the upper laser level [40]. In Pr^{3+}:$LiYF_4$ the excitation channel for the population of the thermally coupled ^3P_J and $^1I_6$ upper laser level multiplets corresponds to a 2ω-OPSL pump wavelength of 479 nm (cf. Fig. 1). At a typical doping concentration for efficient lasing of 0.5 at. %, several decay channels in the visible yield an upper state lifetime of about 40 µs. Among the fluorides the high thermal conductivity of 6 $W/(m \cdot K)$ [41] makes $LiYF_4$ suitable also for high pump powers. Finally, Czochralski-grown crystals with high optical quality are commercially available.

In this Letter, we report on a 2ω-OPSL-pumped Pr^{3+}:$LiYF_4$ laser delivering almost 3 W of output power at slope efficiencies up to 72% with optical-to-optical efficiencies exceeding 60% in the green and the red spectral region. Moreover, we demonstrate the highest output power and slope efficiency on the orange transition at 607 nm with 1.8 W and 60%, respectively. Laser operation on several other transitions was characterized as well.

A schematic of the laser setup used in the experiments is depicted in Fig. 2. The hemispherical v-type resonator consisted of three mirrors, M1–M3. M1 and M2 were plane and highly reflective coated for the respective laser wavelengths. Both had a transmission >99% at the pump wavelength, enabling a high fraction of launched pump power and the measurement of the transmitted pump light during laser operation, which additionally, by accounting for the Fresnel reflections on the crystals' end faces, allowed for an accurate determination of the absorbed pump power. M3 had a radius of curvature of 100 mm and a distance of about 100 mm to M1. For M3 different mirrors with appropriate transmission characteristics for the respective desired laser wavelength were applied. The active medium was a commercially fabricated 5 mm long a-cut Pr^{3+}(0.5 at.%):$LiYF_4$ rod (AC Materials, Inc.) with a diameter of 7 mm and uncoated plane parallel end faces. The crystal was mounted in a passively water-cooled copper holder at room temperature and placed close to M1. Depending on the laser wavelength the respective fundamental transversal modes had a diameter between 90 and 110 µm inside the laser crystal. A linearly polarized 2ω-OPSL (Coherent, Inc.) with an output power of 5 W at 479 nm and $M^2 < 3$ served as the pump source. At this wavelength the crystal had an absorption coefficient of $\approx 4.5\ cm^{-1}$. For polarization control a $\lambda/2$ wave plate was used. A 40 mm lens focused the pump beam into a 35 µm diameter pump spot close to the center of the laser crystal. At its surfaces the diameter increased to about 90 µm.

In this setup, cw laser experiments with various output coupling transmissions T_{OC} were carried out at emission wavelengths of 523, 545, 604, 607, 640, 698, and 720 nm. The laser characteristics for the T_{OC} providing the respective highest output powers are depicted in Fig. 3. Almost 3 W could be extracted at 523 and 640 nm at slope efficiencies of 72% and 68% and T_{OC} of 1.4% and 2.3%, respectively. These lasers did not show any thermal rollover even for the highest pump power.

In the orange spectral region the highest slope efficiency was 60% at a wavelength of 607 nm with $T_{OC} = 14.3\%$ (not shown in Fig. 3). However, at pump power levels exceeding 3 W additional emission at 604 nm could be observed. Furthermore, a strong rollover occurred at a comparably low absorbed pump power of 2 W, limiting the maximum output power in this configuration to 1.4 W. At a lower T_{OC} of 5.8% the slope efficiency dropped to 48%, but thermal effects vanished and the maximum power was increased to 1.8 W. Due to the lack of suitable mirrors no T_{OC} between 5.8% and 14.3% could be applied, though even better performance might be expected. Both orange lasers at 607 and 604 nm operated best at comparably high T_{OC} to overcome internal losses originating in ground state absorption into the $^1D_2$ level. Though this transition is spin forbidden and nonresonant, thus exhibiting low cross sections, it is not negligible and impedes efficient lasing in particular at low T_{OC}.

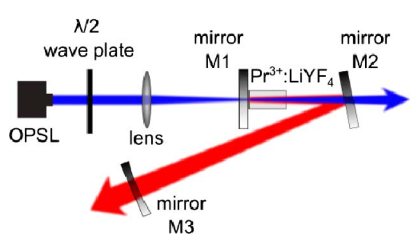

Fig. 2. Schematic of the v-type laser setup used for the experiments.

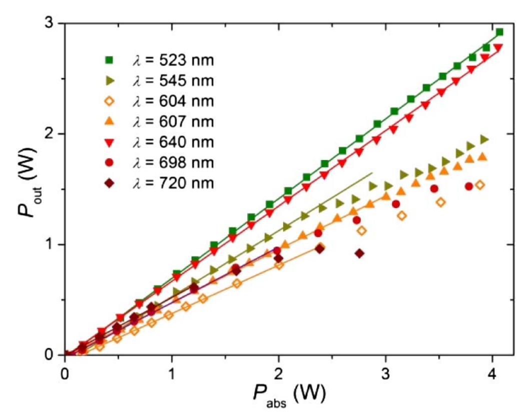

Fig. 3. Input–output characteristics of the Pr^{3+}:$LiYF_4$ lasers at emission wavelengths of 523, 545, 604, 607, 640, 698, and 720 nm. The respective T_{OC} can be found in Table 1.

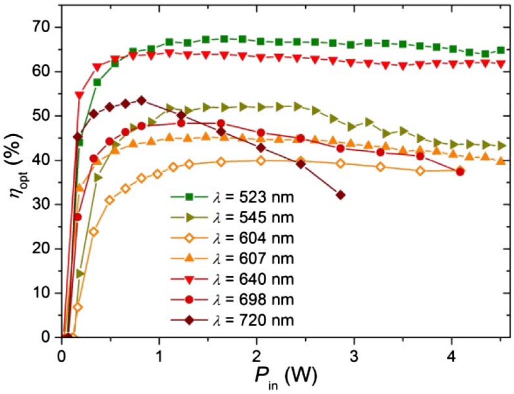

Fig. 4. Optical-to-optical efficiencies of the Pr^{3+}:$LiYF_4$ lasers calculated with respect to the incident pump power.

The lower Stokes efficiency of the lasers with longer emission wavelengths at 698 and 720 nm led to a strong thermal rollover of the efficiency at high pump powers. The beam quality factors M^2 were determined to be <1.5 for the four lasers with the highest output power at maximum pump power. Due to the high absorption efficiency of almost 90% and the low absorbed pump powers P_{thr} at the laser threshold, the maximum optical-to-optical efficiencies η_{opt} even with respect to the incident pump power nearly equal the slope efficiencies. The highest η_{opt} of 67% was obtained for the green laser at 523 nm. The high efficiency and thermal stability of this laser might be surprising regarding the low emission cross section of the corresponding transition. However, it provides the highest Stokes efficiency and thus the lowest heat generation. Furthermore, it emits from a higher level within the thermally coupled ^3P_J and $^1I_6$ multiplets (see Fig. 1), which could lead to increased effective cross sections at higher temperatures, making the laser even benefit from moderate heating.

Figure 4 depicts the evolution of η_{opt} versus the incident pump power for the lasers shown in Fig. 3. The apparent decrease at high pump powers for 523 and 640 nm is actually due to a decreased absorption efficiency that could originate in a temperature-induced decrease of the absorption peak at 479 nm as well as a slight shift in the emission wavelength of the 2ω-OPSL toward higher power. For the other lasers, thermal problems become evident with increasing pump power.

For all lasers except the orange, we estimated the internal roundtrip losses $2\gamma_{int}$: The energy conservation law allows determining a maximum $2\gamma_{int}$ for every T_{OC} according to

$$2\gamma_{int} \leq -\ln(1 - T_{OC}) \cdot \left(\frac{\eta_{Stokes}}{\eta_{sl}} - 1\right), \qquad (1)$$

where $2\gamma_{int}$ must be lower than the minimum value for all T_{OC}. A value as low as 0.2% results for 640 nm (see Table 1), revealing the high optical quality of the laser crystal. While the increased losses toward shorter wavelengths might be attributed to increased Rayleigh-scattering, the higher values at longer wavelengths are caused by the visibly lower surface quality of the mirrors applied in this case. For the orange lasers a calculation according to Eq. (1) does not result in reasonable values due to the $^3H_4 \rightarrow {}^1D_2$ absorption at the laser wavelength. However, the losses are estimated to be in the same order as for the laser at 640 nm. A summary of the parameters of the characterized lasers is given in Table 1.

According to the rate equations a higher T_{OC} should result in higher slope efficiency. However, the increased inversion necessary to reach the threshold might result in detrimental effects such as upconversion. Furthermore, the increased laser threshold itself might cause detrimental thermal effects. In fact we observed a decreased efficiency at high T_{OC} in our experiments. To distinguish between thermal effects, which could be avoided by a more sophisticated cooling, and unavoidable losses resulting from higher inversion levels we recorded the laser characteristics under 500 Hz 1:1 chopped excitation, thus 50% reduced thermal load. Moreover, the slope efficiencies were derived at the lowest pump powers that would still allow for a reliable determination of the gradient of the laser curve. While for the 546 nm transition not enough different T_{OC} were available, we also excluded the mirrors with $T_{OC} = 1.4\%$ for 523 nm and 2.3% for 640 nm due to their obviously better quality compared to other mirrors, which would have falsified the following considerations.

The resulting curves are depicted in Fig 5. Despite our efforts to minimize thermal load, all lasers other than the orange ones exhibit a maximum slope efficiency at comparably low T_{OC} between 2% and 6% and η_{sl} drops significantly at higher T_{OC}. For the orange lasers, the slope efficiency reaches a maximum at significantly higher T_{OC} due to the additional ground state absorption losses dominating at low T_{OC}. The maximum η_{sl} is also lower, because inversion dependent losses are already significant at this T_{OC}. This can be seen by comparison with the 640 nm laser, which has higher cross sections and thus even lower inversion at the same T_{OC}. In conclusion, Pr^{3+}:$LiYF_4$ seems to be prone to inversion dependent

Table 1. Laser Parameters of the 2ω-OPSL-Pumped Pr^{3+}:$LiYF_4$ Lasers[a]

λ_{em} (nm)	$\sigma_{em}(10^{-20}\ cm^2)$	T_{OC} (%)	P_{thr} (mW)	P_{max} (W)	η_{sl} (%)	$\eta_{opt,max}$ (%)	$2\gamma_{int}$ (%)	M^2 at P_{max}
523	2.6	1.4	52	2.9	72	67	0.4	<1.1
546	0.8	2.4	120	2.0	60	52	0.3	<1.5
604	9.8	11.1	114	1.5	44	40	(0.2)	—
607	13.6	5.8	26	1.8	48	45	(0.2)	<1.4
607	13.6	14.8[b]	185	1.4	60	45	(0.2)	—
640	21.8	2.3	17	2.8	68	64	0.2	<1.2
698	5.2	5.8	65	1.5	50	48	0.6	—
720	8.8	2.7	16	1.0	53	53	0.4	—

[a]Note: The respective laser curves can be found in Fig. 3. The numbers in parentheses are estimates.
[b]Not shown in Fig. 3.

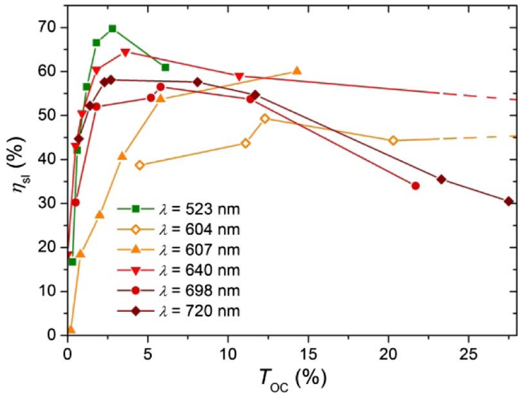

Fig. 5. Dependency of the slope efficiency on the output coupling transmission for quasi-cw Pr^{3+}:$LiYF_4$ lasers operated at different wavelengths.

losses and thus has to be operated at comparatively low T_{OC}. Achieving highest efficiencies under these conditions thus requires very high-quality crystals. Even small resonator losses will lead to a drop of the achievable maximum slope efficiency. Further experiments are necessary to prove and quantify this hypothesis.

In conclusion, we presented 2ω-OPSL-pumped Pr^{3+}:$LiYF_4$ lasers with record high slope efficiencies of 72% and 68% at wavelengths of 523 and 640 nm, respectively, with maximum output powers close to 3 W. Furthermore, we were able to significantly improve the slope efficiency of the orange laser at 607 nm to 60%. Slope efficiencies between 40% and 60% and output powers exceeding 1 W were presented for four other laser wavelengths. Our results prove that the most efficient high-power laser operation of Pr^{3+}:$LiYF_4$ requires very high-quality laser crystals, because the maximum possible efficiency decreases at increased inversion densities resulting from a higher T_{OC} needed to compensate for intracavity losses from imperfect crystals. Further investigations are necessary to quantify this effect and to find the optimum configuration of doping level, cooling scheme, and output coupling rate for each wavelength.

We are very grateful for the financial support by the Deutsche Forschungsgemeinschaft within the graduate school 1355 "Physics with new advanced coherent light sources."

References

1. J.-A. Conchello and J. W. Lichtman, Nat. Methods **2**, 920 (2005).
2. S. Engler, R. Ramsayer, and R. Poprawe, Phys. Procedia **12**, 339 (2011).
3. T. H. Maiman, Nature **187**, 493 (1960).
4. A. Yariv, S. P. S. Porto, and K. Nassau, J. Appl. Phys. **33**, 2519 (1962).
5. R. Solomon and L. Mueller, Appl. Phys. Lett. **3**, 135 (1963).
6. F. Varsanyi, Appl. Phys. Lett. **19**, 169 (1971).
7. T. Sandrock, T. Danger, E. Heumann, G. Huber, and B. H. T. Chai, Appl. Phys. B **58**, 149 (1994).
8. T. Danger, A. Bleckmann, and G. Huber, Appl. Phys. B **58**, 413 (1994).
9. E. Heumann, C. Czeranowsky, T. Kellner, and G. Huber, in *Conference on Lasers and Electro-Optics*, OSA Technical Digest (Optical Society of America, 1999), p. 86.
10. S. Ruan, J. M. Sutherland, P. M. W. French, J. R. Taylor, and B. H. T. Chai, Opt. Lett. **20**, 1041 (1995).
11. J. M. Sutherland, P. M. W. French, J. R. Taylor, and B. T. H. Chai, Opt. Lett. **21**, 797 (1996).
12. J. Y. Allain, M. Monerie, and H. Poignant, Electron. Lett. **27**, 1156 (1991).
13. S. C. Goh, R. Pattie, C. Byrne, and D. Coulson, Appl. Phys. Lett. **67**, 768 (1995).
14. E. Osiac, E. Heumann, G. Huber, S. Kück, and E. Sani, Appl. Phys. Lett. **82**, 3832 (2003).
15. R. G. Smart, D. C. Hanna, A. C. Tropper, S. T. Davey, S. F. Carter, and D. Szebesta, Electron. Lett. **27**, 1307 (1991).
16. S. Nakamura, M. Senoh, S.-I. Nagahama, N. Iwasa, T. Yamada, H. Kiyoku, and Y. Sugimoto, Jpn. J. Appl. Phys. **35**, L74 (1996).
17. A. Richter, E. Heumann, E. Osiac, G. Huber, W. Seelert, and A. Diening, Opt. Lett. **29**, 2638 (2004).
18. M. Fibrich, H. Jelínkova, J. Šulc, K. Nejezchleb, and V. Škoda, Appl. Phys. B **97**, 363 (2009).
19. P. Camy, J. L. Doualan, R. Morcorgé, J. Bengoechea, and U. Weichmann, Opt. Lett. **32**, 1462 (2007).
20. U. Weichmann, J. Baier, J. Bengoechea, and H. Moench, in *European Conference on Lasers and Electro-Optics and the International Quantum Electronics Conference* (IEEE, 2007), paper CJ-347.
21. A. Giesen, H. Hügel, A. Voss, K. Wittig, U. Brauch, and H. Opower, Appl. Phys. B **58**, 365 (1994).
22. http://www.coherent.com/http://www.coherent.com/Products/?1891/Genesis-Taipan-460-nm-to-577-nm.
23. M. Kuznetsov, F. Hakimi, R. Sprague, and A. Mooradian, IEEE Photon. Technol. Lett. **9**, 1063 (1997).
24. A. Richter, H. Scheife, E. Heumann, G. Huber, W. Seelert, and A. Diening, Electron. Lett. **41**, 794 (2005).
25. E. Osiac, E. Heumann, A. Richter, G. Huber, A. Diening, and W. Seelert, in *Conference on Lasers and Electro-Optics*, OSA Technical Digest (Optical Society of America, 2004), paper CFE2.
26. V. Ostroumov and W. Seelert, Proc. SPIE **6871**, 68711K (2008).
27. F. Reichert, D.-T. Marzahl, P. Metz, M. Fechner, N.-O. Hansen, and G. Huber, Opt. Lett. **37**, 4889 (2012).
28. F. Reichert, T. Calmano, S. Müller, D.-T. Marzahl, P. W. Metz, and G. Huber, Opt. Lett. **38**, 2698 (2013).
29. F. Starecki, W. Bolaños, A. Braud, J.-L. Doualan, G. Brasse, A. Benayad, V. Nazabal, B. Xu, R. Moncorgé, and P. Camy, Opt. Lett. **38**, 455 (2013).
30. L. Esterowitz, R. Allen, M. Kruer, F. Bartoli, and L. S. Goldberg, J. Appl. Phys. **48**, 650 (1977).
31. B. Xu, P. Camy, J.-L. Doualan, Z. Cai, and R. Moncorgé, Opt. Express **19**, 1191 (2011).
32. B. Xu, Z. Liu, H. Xu, Z. Cai, C. Zeng, S. Huang, Y. Yan, F. Wang, P. Camy, J.-L. Doualan, A. Braud, and R. Moncorgé, Opt. Commun. **305**, 96 (2013).
33. M. Malinowski, M. F. Joubert, and B. Jacquir, Phys. Status Solidi A **140**, K49 (1993).
34. T. T. Basiev, V. A. Konyushkin, D. V. Konyushkin, M. E. Doroshenko, G. Huber, F. Reichert, N.-O. Hansen, and M. Fechner, Opt. Mater. Express **1**, 1511 (2011).
35. F. Reichert, F. Moglia, D.-T. Marzahl, P. Metz, M. Fechner, N.-O. Hansen, and G. Huber, Opt. Express **20**, 20387 (2012).
36. H. Okamoto, K. Kasuga, I. Hara, and Y. Kubota, Opt. Express **17**, 20227 (2009).
37. P. W. Metz, S. Müller, F. Reichert, D.-T. Marzahl, F. Moglia, C. Kränkel, and G. Huber, Opt. Express **21**, 31274 (2013).
38. V. Lupei, N. Pavel, and T. Taira, Appl. Phys. Lett. **83**, 3653 (2003).
39. T. Gün, P. Metz, and G. Huber, Opt. Lett **36**, 1002 (2011).
40. J. Hegarty, D. L. Huber, and W. M. Yen, Phys. Rev. B **25**, 5638 (1982).
41. B. W. Woods, S. A. Payne, J. E. Marion, R. S. Hughes, and L. E. Davis, J. Opt. Soc. Am. B **8**, 970 (1991).